steel research international
www.steel-research.de

On the Role of Tramp Elements for Surface Defect Formation in Continuous Casting of Steel

Christian Bernhard, Georg Gaiser, Michael Bernhard, Johann Winkler, Maximilian Kern, Peter Presoly, and Youn-Bae Kang*

Dedicated to 150 years of the Institute of Iron– and Steel Technology at the TU Berguniversitaet Freiberg

In the course of the decarbonization of steel production, electric steel production will continue to gain importance. The processing of low-quality scrap will also play an important role, which may lead to an increase in the content of so-called tramp elements in steel production and further processing. This article examines the effect of the elements Cu, Sn, and Ni on the formation of surface cracks under the conditions of the continuous casting process. Results of an in situ bending test are compared with the results of the experimental simulation of high-temperature oxidation and thermodynamic analysis based on the CALculation of PHase Diagrams (CALPHAD) approach. For a temperature of 900 °C, an equivalent Cu content of 0.20 wt% must be considered as the critical upper limit. The presumable reason is the existence of Cu- and Sn-rich liquid phases at the austenite grain boundaries. The results clearly show the effect of the investigated elements but also point to the importance of the gas atmosphere and cooling conditions on the results. This can be a groundbreaking result for extending the process window for casting steels with increased tramp element contents.

C. Bernhard, G. Gaiser, M. Bernhard, M. Kern, P. Presoly
Chair of Ferrous Metallurgy
Montanuniversitaet Leoben
Franz-Josef Strasse 18, 8700 Leoben, Austria
E-mail: christian.bernhard@unileoben.ac.at

M. Bernhard, Y.-B. Kang
Graduate Institute of Ferrous and Eco Materials Technology
Pohang University of Science and Technology
77 Cheongam-Ro, Pohang, Gyung-buk 37673, Korea

J. Winkler
K1-MET GmbH
Stahlstraße 14, Linz 4020, Austria

The ORCID identification number(s) for the author(s) of this article can be found under https://doi.org/10.1002/srin.202400494.

© 2024 The Author(s). Steel Research International published by Wiley-VCH GmbH. This is an open access article under the terms of the Creative Commons Attribution-NonCommercial-NoDerivs License, which permits use and distribution in any medium, provided the original work is properly cited, the use is non-commercial and no modifications or adaptations are made.

DOI: 10.1002/srin.202400494

1. Introduction

The ongoing trend toward the decarbonization of steel production, with the main emphasis on reducing climate-damaging emissions, will impact the input of raw materials into iron- and steelmaking and may shift the operation points concerning residuals and tramp elements in steel. As one scenario, the increased use of low-grade scrap could lead to an increase in the content of harmful elements such as Cu and Sn in the produced steel, to name just two examples. The negative impact of tramp elements on the mechanical properties of steel was already widely studied in detail in the 1990s during the first phase of replacing integrated steel production with electric arc furnaces.[1–5]

However, the understanding of the effect of tramp elements on surface quality in the continuous casting process is based on only a few fundamental studies, some of which were already carried out in the 1960s–1980s.[6–10] Wolf[10] identified tramp elements, such as Cu, as the cause for the formation of fine network cracks on the strand surface. The enrichment of Cu and the formation of low-melting liquid phases along the austenite grain boundaries as a result of selective oxidation and due to the negative impact of ferrite-forming elements such as Sn, Sb, and As were the most commonly given explanation for a higher crack susceptibility at temperatures between 1100 °C and 1200 °C. In addition, the positive effect of Ni has already been described in these early publications. The decrease of the solubility of Cu in austenite by Sn and conversely the increase of solubility due to Ni was investigated by several authors,[11–13] resulting in the formulation of a characteristic value to prevent the formation of fine network cracks, the critical "Cu-equivalent." In the most common form, the Cu-equivalent is defined either as

$$\mathrm{Cu_{eq}}[\mathrm{wt\%}] = [\mathrm{wt\%Cu}] + 10[\mathrm{wt\%Sn}] - [\mathrm{wt\%Ni}] - 2[\mathrm{wt\%S}] \tag{1}$$

according to ref. [14] with an empirically determined critical upper limit of 0.25–0.30 wt%, or

 © 2024 The Author(s). Steel Research International published by Wiley-VCH GmbH

$$Cu_{eq}[wt\%] = [wt\%Cu] + 6[wt\%Sn + wt\%Sb] - [wt\%Ni] \quad (2)$$

according to ref. [7] with a critical Cu_{eq} of 0.40 wt%.

The presumed ductility trough at 1100–1200 °C caused by exceeding the critical Cu-equivalent was postulated by Wolf[9] but never confirmed by hot tensile tests. Comineli et al.[15] have summarized the results from several publications on hot tensile tests and identified the segregation of Cu toward grain boundaries, a possible interaction with MnS, and deformation-induced precipitation of fine Cu_2S as causes for a lower ductility. Actually, hot tensile tests commonly show only a moderate decrease in the reduction-of-area with increasing Cu and Sn content.[16] The most presumable reason is that heat treatment before the tensile test is usually performed under oxidation protection by inert gases. Under these conditions, oxidized grain boundaries do not become the nuclei for the formation of cracks. Imai et al.[17] conducted interrupted hot tensile after oxidation of the samples and counted the number of defects on the sample surface. From the experimental results, a negative impact of Cu and Sn ($Cu_{eq} = 0.7$ wt %) and a positive influence of Ni became obvious at 1100 °C. In another work, P, Si, B, and C were also found to reduce the susceptibility to surface hot shortness by restraining the penetration of the Cu-enriched phase along grain boundaries.[18] External oxidation at higher temperatures was also identified to have a positive influence, while coarse grains promote hot shortness.

The present work attempts to question the extent to which newly developed experiments and current thermodynamic databases can contribute to a better understanding of the influence of the tramp elements Cu, Sn, and Ni on the formation of surface defects in casting and rolling processes and to conclude on possible counteractions, including modification of steel composition or a change of casting parameters. The investigations are based on "in situ material characterization by bending" (IMC-B) tests[19,20] with increased content of Cu, Sn, and Ni. High-temperature thermal gravimetry will provide a detailed view of external and internal oxidation behavior under the thermal conditions of casting, reheating, and rolling. Finally, thermodynamic considerations on the formation of low melting eutectics in the system Cu and Sn will supplement the examinations carried out and provide an insight into the mechanisms of hot shortness due to tramp elements.

2. Materials and Methods

2.1. IMC-B Test

The IMC-B test is a well-established tool for investigating the effect of alloying additions, thermal cycles, bending temperature, deflection, and bending rate on surface defect formation.[19–25] The results provide a conclusion on critical strain to prevent defect formation. So far, the influence of C, Si, Al, and Nb has been the focus of recent investigations carried out. A significant difference to classic hot tensile tests relies on the test procedure, i.e., cooling and bending, under an oxidizing atmosphere. Both air and air/water vapor mixtures can be set as the ambient atmosphere. The resulting grain boundary segregations and grain boundary oxide films represent a weak point for the subsequent deflection of the sample and lead to the initiation of surface cracks at low tensile strains. The influence of the cooling cycle, i.e., the oxidation conditions, on the bending test result is remarkable and provides a conclusion on the importance of initial solidification and cooling in the mold on surface defect formation in the straightening zone.

The IMC-B test comprises the following sequence of test steps:[19–25] steel with a specified chemical composition is melted in an induction furnace and then cast into a steel mold, split into two parts. The sample with dimensions 180 × 58 × 24 mm is then cooled similarly to the provided temperature profile of a continuous casting machine[26,27] under air or an air/water vapor mixture. The temperature of the sample is monitored by optical measurement. After a predetermined cooling time, the sample is placed in a heated bending furnace, homogenized, and bent slowly and with low deflection. After cooling to room temperature, the sample is descaled, and the cracks on the surface are counted and measured using a digital microscope. The procedure of the IMC-B test is illustrated in **Figure 1**.

Within this article, the results of ten bending tests on a typical medium carbon steel with different Cu, Sn, and Ni contents are presented and discussed in detail. **Table 1** shows the chemical composition of these ten experiments. Except for Cu, Sn, and Ni, the chemical composition is remained constant. The average N content is below 80 ppm in all samples. Steel 0 represents the reference composition. For steels 1 and 2, either Cu or Sn is

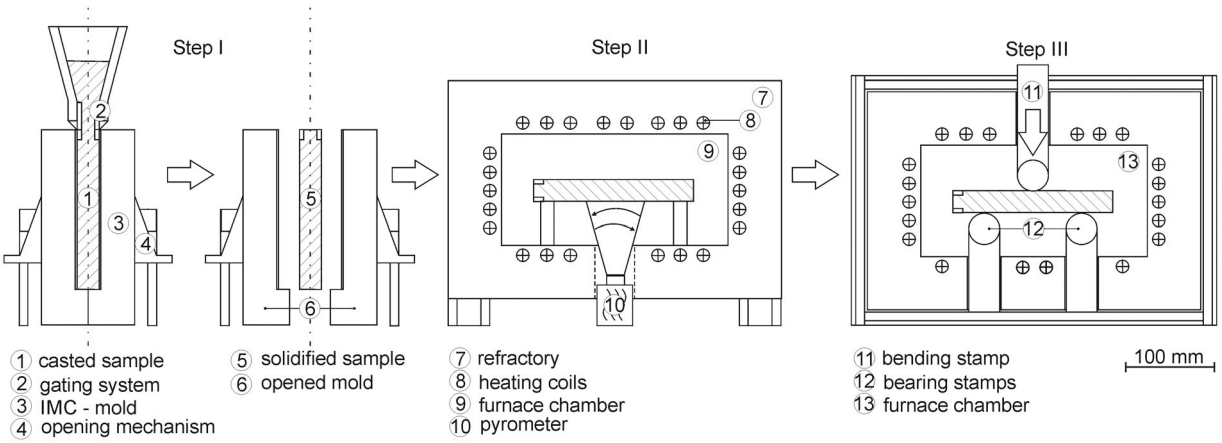

Figure 1. Schematic illustration of the IMC-B test. Reproduced under the CC-BY 4.0 license.[20]

© 2024 The Author(s). Steel Research International published by Wiley-VCH GmbH

1869344x, 0, Downloaded from https://onlinelibrary.wiley.com/doi/10.1002/srin.202400494 by Readcube (Labtiva Inc.), Wiley Online Library on [11/10/2024]. See the Terms and Conditions (https://onlinelibrary.wiley.com/terms-and-conditions) on Wiley Online Library for rules of use; OA articles are governed by the applicable Creative Commons License

Table 1. Chemical composition of the tested steel grades, all values in wt%.

Steel	Chemical composition [wt%]									
	C	Mn	Si	P	S	Al	Cu	Sn	Ni	Cu_{eq}
Steel 0							<0.013	<0.002	<0.008	<0.025
Steel 1							0.15	<0.002	<0.008	0.15
Steel 2							<0.017	0.015	<0.008	0.16
Steel 3							0.25	0.028	<0.009	0.52
Steel 4							0.22	0.027	0.09	0.39
Steel 5	0.17	1.59	0.43	0.01	0.003	0.029	0.16	0.010	<0.008	0.24
Steel 6							0.16	0.012	<0.002	0.28
Steel 7							0.15	0.008	0.11	0.12
Steel 8							0.17	0.011	0.26	0.02
Steel 9							0.15	0.01	0.20	0.05
Steel 10							0.16	0.02	0.36	0

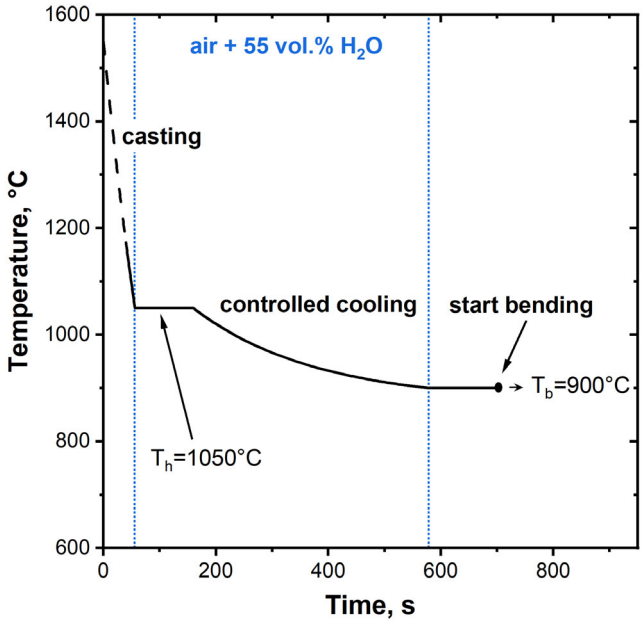

Figure 2. Temperature cycle and characteristic time points in the test sequence.

added, whereas steels 3, 5, and 6 show a specific variation of Cu and Sn. Steels 4, 7–10 represent alloys with a changing Cu and Sn content but with increasing Ni level. The last column provides the calculated Cu equivalent Cu_{eq} according to Equation (1). The values range from 0 to 0.52 wt%.

The reference steel grade shows a pronounced crack susceptibility at a bending temperature of 900 °C.[19–21] Therefore, the thermal cycle, according to **Figure 2** (data given in **Table 2**), was selected for the present IMC-B-experiments: the exit temperature from the mold after 45 s is roughly 1180 °C. A temperature holding step at 1050 °C is adjusted till a total time of 160 s before the sample is cooled to the bending temperature of 900 °C. Homogenization and cooling are performed in a chamber furnace purged with air and steam with an approximate concentration of 55 vol% water vapor. The gas composition is adjusted by the humidification of compressed air. All gas lines are heated to 200 °C to avoid condensation after humidification. The total gas volume at the respective furnace temperature corresponds to a maximum value of 110 L min^{-1}. The time between the casting and the start of homogenization in the bending furnace is adjusted to 580 s. The homogenization ends after 700 s. Finally, the bending takes 175 s, with 125 s for loading and 50 s for unloading. Both homogenization and bending are conducted under air. In total, the experiment takes 875 s, which characterizes the typical casting time until straightening in a slab caster. The vertical blue lines in Figure 2 indicate the time range where a water vapor-based atmosphere is applied.

To simulate controlled straightening, the sample is subjected to a three-point bending test after thermal homogenization of the sample. Bending is performed in a heated furnace under isothermal conditions. The lowering speed of the bending punch and the maximum lowering are specified and, according to the

Table 2. Experimental parameters for the IMC-B tests.

Mold cooling [s]	T after mold [°C]	T holding step [°C]	t after holding [s]	t after cooling to bending temperature [s]	Water vapor content of the ambient atmosphere[vol%]
45	≈1180	1050	160	580	55 ± 5
t bending start – end [s]			Maximum strain [%]		Strain rate [s^{-1}]
700–875			6		$4.7.10^{-4}$

© 2024 The Author(s). Steel Research International published by Wiley-VCH GmbH

1869344x, 0, Downloaded from https://onlinelibrary.wiley.com/doi/10.1002/srin.202400494 by Readcube (Labtiva Inc.), Wiley Online Library on [11/10/2024]. See the Terms and Conditions (https://onlinelibrary.wiley.com/terms-and-conditions) on Wiley Online Library for rules of use; OA articles are governed by the applicable Creative Commons License

3D-finite element simulation of the bending with a visco-elastoplastic approach,[22] result in a maximum tensile strain of 6.0% along the bending axis and a strain rate of $4.7.10^{-4}$ s^{-1}, which comes close to the straightening operation in slab casting.[22] After cooling the samples to room temperature, the samples are descaled by diluted citric acid. The area of 40 mm to the left and right of the bending axis is divided into segments of 5 × 15 mm across the entire width of the specimen. Digital microscopy (Keyence VHX7000) provides the number of defects per segment, as well as the length and depth of each defect.[20] A characteristic bending stress is assigned to each segment depending on its distance from the bending axis, and the segment where cracks first occur provides the critical strain ϵ_C. **Figure 3** exemplarily shows the crack analysis for steel 10. Figure 3a indicates the sum of the number of cracks detected over all segments across the width of the specimen at a distance from the bending axis and the associated normal distribution. The calculated bending strain over the distance from the bending axis is shown in Figure 3b. Assuming two defects per segment are the critical value, the critical strain of around 3.8% can be concluded. According to the literature, the straightening strain typically amounts to 1.0–2.0%.[28,29] To consider a certain degree of safety in the critical value, in the following, a critical elongation of less than 2% is considered critical at a straightening temperature of 900 °C. Hence, the results of steel 10 demonstrate a rather uncritical behavior at 900 °C.

2.2. High-Temperature Oxidation Experiments

An increasing content of tramp elements could lead to critical impact on the grain boundaries while reheating, annealing, or galvanizing. The use of hydrogen or inductive heating instead of natural gas could also change the operating points for heating and rolling with respect to product quality. These aspects have prompted the development of a new experimental setup for investigating high-temperature oxidation of steel during the last few years, consisting of a Netzsch STA 449 F3 Jupiter with a water vapor furnace and a differential thermal analysis and thermogravimetry (DTA-TG) sample carrier, a water vapor generator aSteam DV-2, and an additional tube furnace (Nabertherm RD30A173A) to ensure improved inert heating and cooling of the samples. Samples with dimensions of 13 × 12.2 mm and a thickness of 2 mm were prepared by a wet abrasive cutting machine ATM Brilliant 220. A hole measuring 2.5 mm diameter was drilled to secure the suspended specimen. To avoid contaminations of the sample, a cleaning step with ethanol and acetone was performed right before the experiment. The evaluation of first results and additional information can be found in references.[24,25,30]

Based on this setup, it is possible to address complex issues such as the simulation of processes, which includes temperature control, the adjustment of both inert and oxidizing gas atmosphere during the experiment, and the adjustment of the purging gas composition according to the conditions in the simulated process. **Figure 4** schematically shows the test conditions for the simulation of oxidation in the IMC-B-test as described above: heating and subsequent homogenization take place up to 1200 °C in an inert atmosphere. After setting the initial temperature of 1175 °C, the test conditions change to an oxidizing atmosphere; either controlled cooling under syn. air (synthetic air, 80 vol% N_2 and 20 vol% O_2) or a mixture of syn. air and 50 vol% of water vapor are used for the experiments. Isothermal holding at 900 °C is then carried out in the syn. air, followed by cooling to room temperature in an inert atmosphere. Depending on the oxidation temperature and gas quantity, the gas velocity for the different oxidation gases in the furnace ranges from 2.98 to 7.35 cm s^{-1}. Thermogravimetry provides the weight gain during the test and allows the reaction kinetics, such as the scaling constant, to be determined. The influence of tramp elements on internal oxidation and grain boundary oxidation is investigated by metallographic examination of the oxidized samples.

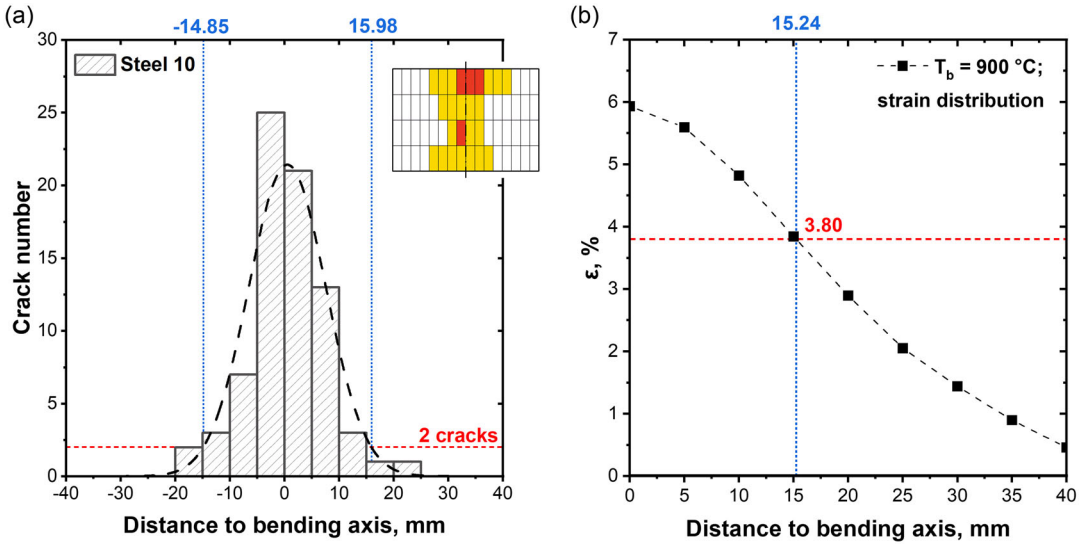

Figure 3. a) Number of defects per segment over the distance to the bending axis with Gaussian distribution and b) calculated tensile strain due to bending for a temperature of 900 °C.

© 2024 The Author(s). Steel Research International published by Wiley-VCH GmbH

1869344x, 0, Downloaded from https://onlinelibrary.wiley.com/doi/10.1002/srin.202400494 by Readcube (Labtiva Inc.), Wiley Online Library on [11/10/2024]. See the Terms and Conditions (https://onlinelibrary.wiley.com/terms-and-conditions) on Wiley Online Library for rules of use; OA articles are governed by the applicable Creative Commons License

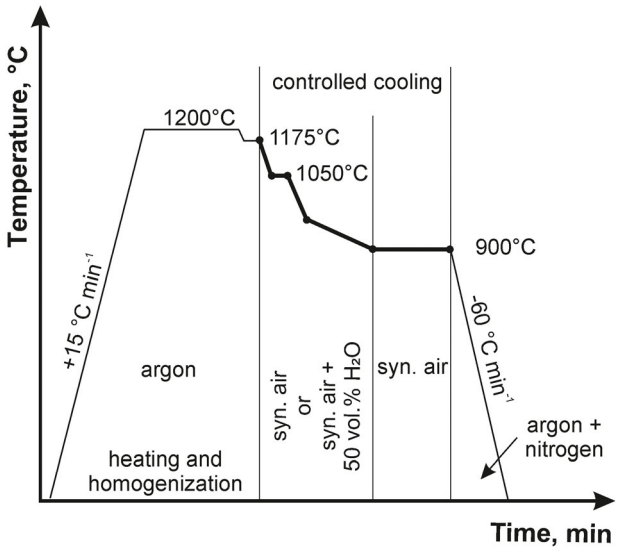

Figure 4. Thermal cycle and main parameters for the performed simulation of the IMC-B test in thermal analysis.

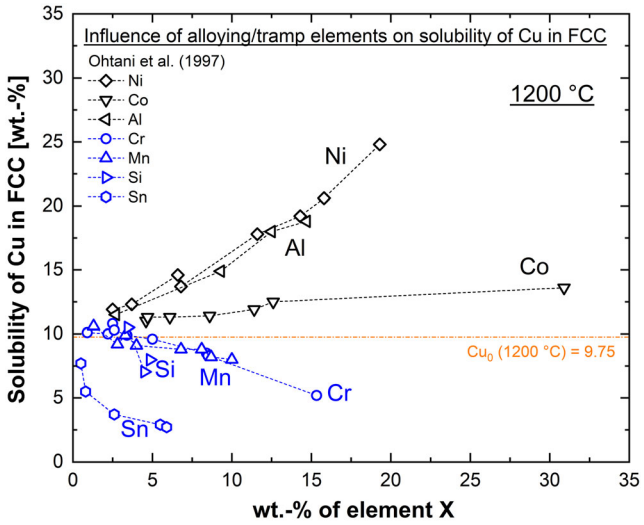

Figure 5. Influence of alloying element X (X = Ni, Al, Co, Si, Mn, Cr, Sn) on the solubility of Cu in austenite (FCC) at 1200 °C. Experimental data are taken from the work of Ohtani et al.[32]

2.3. Thermodynamics and CALculation of PHase Diagrams (CALPHAD)-Type Modeling

In general, the thermodynamics of tramp elements in steel deals with the maximum solubility of Cu in solid face-centered cubic (FCC) austenite before a Cu-rich liquid phase forms. The first experimental phase equilibrium studies on the influence of Sn, As, Sb, Ni, and Mn on Cu solubility in FCC were carried out by Melford[7] and Salter[31] in the 1960s on plain C steels. The observed temperature range was between 900 °C and 1350 °C. It was found that Sn, Sb, and As lead to a significant decrease in Cu solubility, whereas the opposite effect was observed for Ni. A systematic investigation on solid/liquid phase equilibria in ternary Fe–Cu–X (X = Sn, Mn, Si, V, Co, Cr, Al) was carried out by Ohtani et al.[32] who confirmed the previously observed influences of Sn, Ni, and Mn in the temperature range 1100–1300 °C. These results are shown together with those of Al, Co, Cr, and Si at 1200 °C in **Figure 5**. The solubility of Cu in the binary Fe–Cu FCC alloy (Cu_0) at 1200 °C is marked with 9.75 wt%.[33] Of particular interest are the positive effects of Co and Al, which also lead to an increase in the solubility of Cu as it is in the case of Ni. At this point, however, it should be noted that only a limited quantity of data is available, especially for Sn, Sb, or As and their interactions. More detailed investigations as part of the transformation to green steel production on a scrap basis are essential here to provide thermodynamic simulation tools within the CALPHAD framework.[34]

Using the CALPHAD method, thermodynamic databases have recently been developed for a large variety of alloy systems. In this approach, comprehensive experimental data, either from the literature or obtained from own measurements, are used to model the stable phases of one-, two- or three-component systems. The major advantage of the self-consistent CALPHAD databases is the precise extrapolation of the constituent systems to multicomponent alloys and the rapid calculation time achieved with standard thermochemical software packages, e.g., ref. [35].

Regarding the tramp elements in steel, ternary systems such as Fe–Cu–Al,[36] Fe–Cu–Ni,[37] and Fe–Cu–Cr[38] have been successfully modeled in the past. However, due to the lack of experimental information, e.g., for Fe–Cu–Sn, Fe–Cu–Sb, or Fe–Cu–As, only estimates focusing on a specific compositional corner, e.g., Cu,[39] are available or have not been published at all. The following section presents the status of the development of a thermodynamic database[40–42] for accompanying elements in steel, which should be ready for use in the FactSage thermochemical software[35] after completion. A focus was given on the ternary system Fe–Cu–Sn consisting of its binary systems (Fe–Cu, Fe–Sn, and Cu–Sn) and phase equilibria in several isothermal sections of the Fe–Cu–Sn alloys.[31,32] Further, it will be demonstrated in Section 3.2 that additional experimental research is necessary in the future to successfully model the system over the wider composition and temperature ranges.

For the liquid phase, the modified quasi-chemical model (MQM) in the pair approximation[43,44] was used to formulate the Gibbs energy. Pelton and Kang[45] have shown that, compared to the Bragg–Williams random mixing model, the MQM generally provides better results for modeling the Gibbs energy when there is a tendency for short-range order in the melt. The MQM has been successfully used to describe Fe-containing melts in numerous thermodynamic modeling studies, for example, in metal/metal[46,47] and metal/nonmetal[48–50] systems. In the pair approximation for a binary solution consisting of A and B atoms, the following pair-exchange reaction on the sites of a quasi-lattice is considered:

$$(A-A)+(B-B)=2(A-B);\ \Delta g_{AB} \tag{3}$$

where $(i-j)$ is the first nearest neighbor pair and Δg_{AB} represents the nonconfigurational Gibbs free energy change to form 2 mols of $(i-j)$ pairs. The Gibbs energy of the solution is given by

$$G=\left(n_A^o g_A^o+n_B^o g_B^o\right)-T\Delta S^{config}+(n_{AB}/2)\Delta g_{AB} \tag{4}$$

© 2024 The Author(s). Steel Research International published by Wiley-VCH GmbH

1869344x, 0, Downloaded from https://onlinelibrary.wiley.com/doi/10.1002/srin.202400494 by Readcube (Labtiva Inc.), Wiley Online Library on [11/10/2024]. See the Terms and Conditions (https://onlinelibrary.wiley.com/terms-and-conditions) on Wiley Online Library for rules of use; OA articles are governed by the applicable Creative Commons License

with n_A^o and n_B^o are the moles of A and B and g_A^o and g_B^o are the molar Gibbs energies of the pure elements. ΔS^{config} represents the configurational entropy of mixing and Δg_{AB} may be expanded in terms of pairs fractions the X_{AA} and X_{BB}. The extrapolation of the binary descriptions into ternary systems considering geometrical methods[51] offers the possibility to obtain an accurate description of the Gibbs energy of the liquid phase in multicomponent systems. In the present Fe–Cu–Sn liquid alloy, a Tooplike interpolation method was used, setting Fe as an asymmetric component.

For solid phases showing substantial solutions of Fe, Cu and Sn, the compound energy formalism (CEF)[52] was used. In the ternary Fe–Cu–Sn, the CEF was applied to α/δ-ferrite (body-centered cubic, BCC), γ-Fe and ε-Cu (FCC) and $D0_3$ using two sublattices in each case. Exemplarily, considering a sublattice structure $(A,B)_a(C,D)_d$, the molar Gibbs energy according to the CEF is given by:

$$\begin{aligned} G_m = {} & y'_A y''_C G_{A:C} + y'_A y''_D G_{A:D} + y'_B y''_C G_{B:C} + y'_B y''_D G_{B:D} \\ & + aRT\left(y'_A \ln y'_A + y'_B \ln y'_B\right) + bRT\left(y''_C \ln y''_C + y''_D \ln y''_D\right) \\ & + \sum_{i,j,k} y'_i y'_j y''_k L_{i,j:k} + \sum_{i,j,k} y'_k y''_i y''_j L_{k:i,j} \\ & + \sum_{i,j,k,l} y'_i y'_j y''_k y''_l L_{i,j:k,l} + G_m^{mo} \end{aligned} \tag{5}$$

where y'_i and y''_i are the site fractions of component i on one sublattice, $G_{i:j}$ is the Gibbs energy of an end-member, and $L_{i,j:k}$ and $L_{k:i,j}$ are the interaction energies between *i* and *j* when the other sublattice is only occupied by k. $L_{i,j:k,l}$ is the reciprocal parameter representing the interaction among *i,j,k,l*. G_m^{mo} is the contribution due to magnetic ordering in FCC and BCC per mole of atom.[53] Details on the CEF are given in the work of Sundman and Ågren[54] and Hillert[53]

Binary stoichiometric phases with a defined chemical composition were treated as stoichiometric, e.g., Fe_xSn_y and Cu_xSn_y. The molar Gibbs energy can be described by:

$$G_m = H^{\circ}_{298.15} + \int_{298.15}^{T} c_p dT - T\left[S^{\circ}_{298.15} + \int_{298.15}^{T} \left(\frac{c_p}{T}\right) dT\right] \tag{6}$$

where $H^{\circ}_{298.15}$ and $S^{\circ}_{298.15}$ are the enthalpy and the entropy at 298 K, and c_p is the heat capacity.

2.4. Thermal Analysis Techniques: Differential Scanning Calorimetry (DSC) and High-Temperature Laser Scanning Confocal Microscopy (HT-LSCM)

To validate the thermodynamic description of the Fe–Cu–Sn system with own measurements, classic thermal analysis techniques were applied to determine phase equilibria in selected alloys, corresponding to typical compositions of Cu-rich liquid films formed along the austenite grain boundaries in the IMC-B test (Section 2.1 and 3.1). An alloy with 80Cu-10Fe-10Sn (in wt%) was prepared from high-purity starting materials elements. Fe (technically pure, 99.98%), Cu (high-purity wire), and Sn (Alfa Aesar, granules, 99.5%) were weighed in as charge materials according to the mass fractions to a total mass of 1 g. The materials were melted under an Ar 5.0 protective atmosphere in a NETZSCH STA 409PG Luxx with a3 DTA-TG sensor in a 0.3 mL Al_2O_3 crucible. The sample was melted twice to achieve a high homogenization state. As the thermogravimetric signal remained stable during both melting processes, e.g., no change in weight due to oxidation or evaporation, and no reactions with the crucible material occurred, it was assumed that the initial composition of weighting was unchanged.

The measurements of phase equilibrium temperatures were then carried out in a DSC setup of type Pegasus 404F1 (NETZSCH Geraetebau, Germany) with an Rh furnace ($T_{max} = 1650$ °C) and a Pt DSC sensor with type S thermocouples. Al_2O_3 crucibles (85 µL) and lids were used for all experiments; in each trial, the reference was an empty crucible. The protective tube of the Rh furnace was flushed with Ar 5.0 (99.999%) and a Zr getter was placed directly below the sensor to avoid oxidation at elevated temperatures. The calibration of the DSC setup was carried out by measuring the melting points of pure In, BI, Al, Ag, Au, Ni, and Co of NETZSCH's standards. Samples were prepared for a detailed DSC analysis (2.1 × 2.1 × 1.5 mm) and the heating rate was set at 10 °C min^{-1}. As the measured phase transformation temperatures are affected by the applied heating rate, a special algorithm developed by NETZSCH (Tau-R method) was used to recalculate the temperatures at equilibrium from a single measurement. The critical evaluation of the Tau-R method and further applications to Fe-based materials can be found in references.[47,55–57] The analysis of the DSC charts follows the NIST Recommended Practice Guide.[58]

The DSC analysis was combined with a separated thermo-optical analysis using HT-LSCM. In recent decades, HT-LSCM has been become a valuable tool in iron and steel research, including in situ observations of austenite grain growth,[59–61] phase transformations,[62–64] slag metallurgy,[65–67] and steel/slag/inclusion interactions.[68] The combination of DSC and HT-LSCM analyses is a proven method for determining phase diagrams.[56,64,69] The experiments were carried out using an HT-LSCM type VL2000DX-SVF17SP from Lasertec (Yokohama, Japan) with a high-temperature furnace SVF17-SP from Yonekura (Yokohama, Japan). Samples of 5 × 5 × 1.5 mm were produced from the base alloy. The samples were ground and polished in the standard procedure. After placing the samples on the sample holder, the furnace chamber was evacuated and purged with Ar 5.0. The time-temperature program corresponded to the DSC measurements. After reaching the maximum temperature, controlled cooling to room temperature was carried out at a defined cooling rate of − 400 °C min^{-1} under Ar atmosphere.

3. Results and Discussions

3.1. Influence of Cu, Sn, and Ni on Surface Crack Formation: IMC-B and HT-Oxidation Experiments

Figure 6 shows exemplarily micrographs from samples after bending. For the reference steel grade (steel 0), only a limited number of defects formed along the former austenite grain boundaries. The orientation of the cracks is parallel to the bending axis. For steel 6, severe crack formation is visible.

© 2024 The Author(s). Steel Research International published by Wiley-VCH GmbH

1869344x, 0, Downloaded from https://onlinelibrary.wiley.com/doi/10.1002/srin.202400494 by Readcube (Labtiva Inc.), Wiley Online Library on [11/10/2024]. See the Terms and Conditions (https://onlinelibrary.wiley.com/terms-and-conditions) on Wiley Online Library for rules of use; OA articles are governed by the applicable Creative Commons License

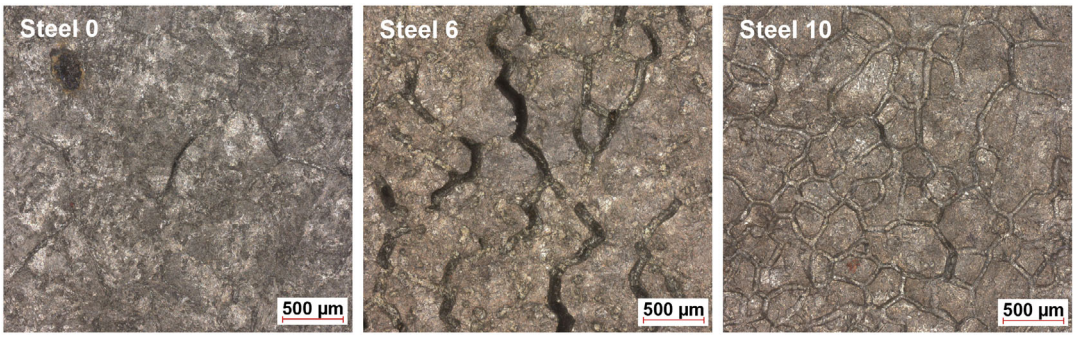

Figure 6. Crack appearance of steel 0, steel 6, and steel 10 around the bending axis.

This type of defect coincides with the well-known network cracks. In the case of steel 10, Ni results in strong oxidation of the former austenite grain boundaries, but only a limited number of cracks are formed.

Another way to graphically display the results of IMC-B tests is a traffic light system. In **Figure 7**, red color marks segments with more than 5 defects, yellow color segments with 1–5 defects, and white color segments without detectable defects. Segments shaded in red are areas with a continuous crack network. For the reference steel grade (steel 0), the critical strain is 2.9%, well above the maximum straightening elongation of 2%. Surprisingly, the addition of 0.15 wt% Cu (steel 1) and 0.015 wt% Sn (steel 2) leads to an improvement in the results: fewer cracks are formed, and the critical strain increases to values above 3%. The simultaneous addition of Cu and Sn, in contrast, leads to a massive deterioration in the specimen's behavior in the bending test: In test no. 3 and 4 ($Cu_{eq} > 0.39$ wt%), the number of defects formed increases dramatically, and the critical elongation drops to values below 0.50%. In tests 5 and 6, both with Cu equivalent of 0.28 and 0.24 wt%, respectively, fewer defects form, but the critical elongation is always less than 1.2% and thus in a very critical range. The addition of Ni achieves a significant improvement. Tests 7 to 10 with a Ni content of up to 0.36 wt% and the corresponding copper equivalent of 0.12, 0.05, and 0 wt% lead to the formation of a smaller number of cracks and increase the critical elongation again to values of 2.6–4.0%.

Figure 8 summarizes the predicted critical strain values for the performed experiments versus the calculated Cu equivalent according to Wolf.[14] The results indicate that a Cu_{eq} of 0.20 wt% should mark the critical range for network crack formation due to tramp elements. The influence of nickel is remarkable, but even adding only a small amount of Ni significantly improves the behavior. The influence of Cu, Sn, and Ni is very well reflected in Wolf's formula; only the critical copper equivalent for the selected conditions is slightly below the value of

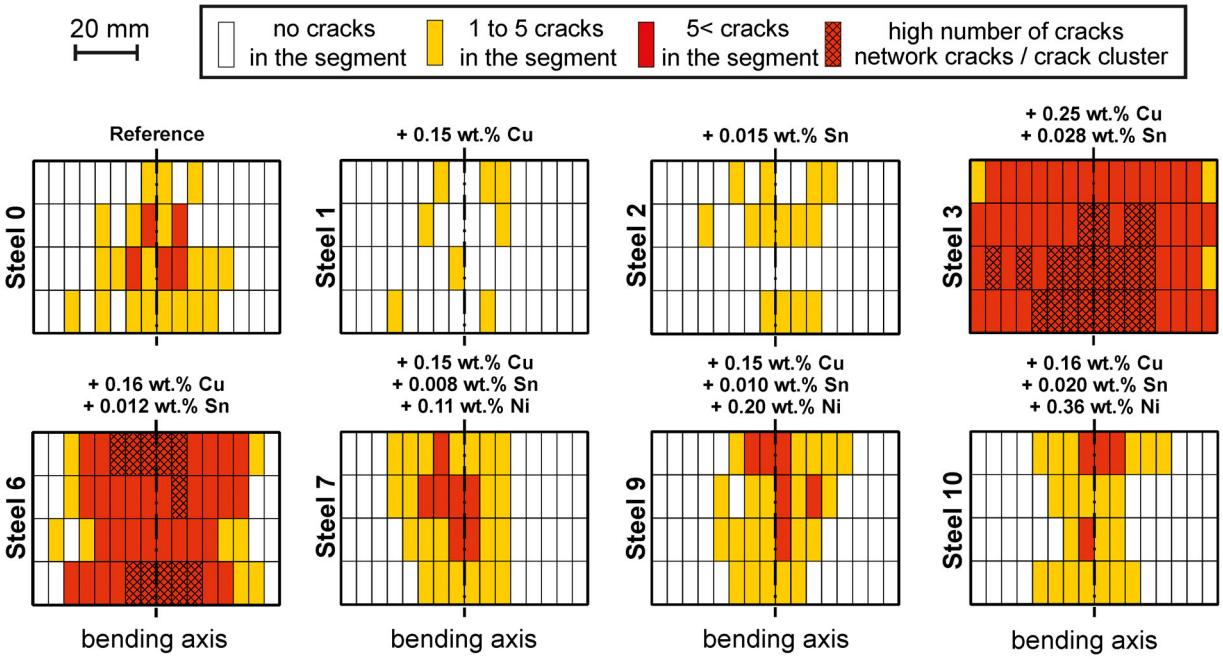

Figure 7. Results of the bending tests in a traffic light system; the colors mark the number of defects per segment.

© 2024 The Author(s). Steel Research International published by Wiley-VCH GmbH

1869344x, 0, Downloaded from https://onlinelibrary.wiley.com/doi/10.1002/srin.202400494 by Readcube (Labtiva Inc.), Wiley Online Library on [11/10/2024]. See the Terms and Conditions (https://onlinelibrary.wiley.com/terms-and-conditions) on Wiley Online Library for rules of use; OA articles are governed by the applicable Creative Commons License

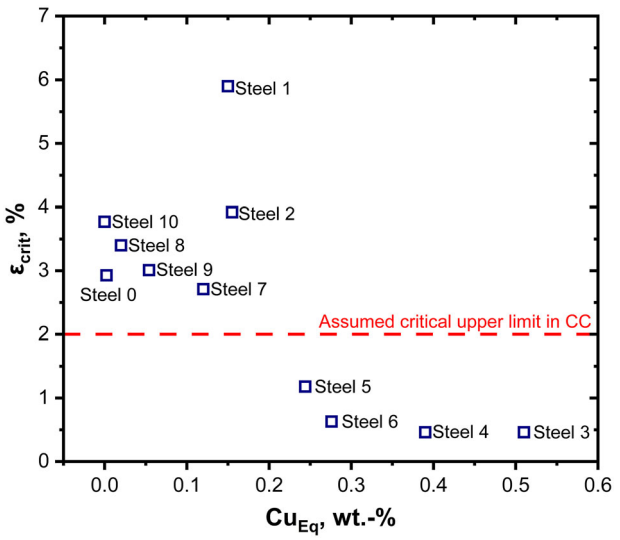

Figure 8. Calculated critical strain from the IMC-B-experiments at 900 °C for all experiments versus the Cu-equivalent according to Equation (1).

0.25–0.30 wt% given by Wolf.[14] An absolute novelty, however, is the influence of tramp elements at bending temperatures of 900 °C. Until now, reduced ductility was mostly attributed to the temperature range of 1100 °C and, hence, temperatures above the melting point of Cu. The clear effect at 900 °C would require the explanation that phases with a melting point below 900 °C are formed due to grain boundary oxidation.

Figure 9 shows a qualitative mapping for steel 3 ($Cu_{eq} > 0.50$ wt%). In the interface area and along the grain boundary, the enrichment of Cu and Sn is clearly visible. In addition, a few Cu-rich particles are occluded in the scale. Scanning electron microscopy/energy dispersive X-ray spectroscopy (SEM/EDS) measurement indicates a Cu concentration of ≈80 wt%, 10 wt% Sn and ≈6 wt% Fe. For this composition, a first thermodynamic calculations using FactSage software[35] predict a melting point of less than 900 °C, confirming the conclusions from the results of the bending tests. Surface oxidation seems thus the key to understanding the mechanisms of oxidation of Cu and Sn-containing steel under oxidizing conditions.

In the following, the results of the high-temperature oxidation experiments about the IMC-B test are illustrated. **Figure 10** provides images from a SEM: on the right side, the interface of a steel 4, and on the left side from steel 3. Generally, adding water vapor to the gas atmosphere accelerates oxidation. For the two tested steel grades, the Ni-containing shows a significantly lower oxidation rate.[70] Low oxidation rates favor internal oxidation, and higher oxidation rates favor external oxidation. Thus, stronger external oxidation lowers the yield but may prevent the negative impact of grain boundary oxidation.[24,30] For the steel without Ni addition, Cu- and Sn-rich phases form to a smaller extent along the grain boundaries but preferably at the interface, thus being of less importance for later surface defect formation. Nevertheless, the small number of damaged grain boundaries seems sufficient to impact the behavior of these steel grades in the IMC-B test. In the case of the Ni-alloyed steel, Cu and Sn remain in the solution, whereas Si and Al mainly control the oxidation. It is important to note that these oxidized grain boundaries may also later on become the nuclei for the growth of surface defects, as presented in a recent publication by the authors.[24] The steel will, therefore, in the IMC-B test, not be free from defects after bending but behave like the reference steel grade without Cu, Sn, and Ni addition.

The adjustment of the gas atmosphere in combination with steel composition and thermal cycling may hence be the key to controlling the behavior of steel with elevated content of tramp elements in casting, reheating, and hot rolling. Ni clearly increases the solubility of Cu and Sn and thus prevents the formation of Cu- and Sn-rich phases at the grain boundaries. However, grain boundaries are also attacked by O in the presence of Ni and can later lead to a quality problem. The last remaining question to answer is if the Cu- and Sn-rich phases may be liquid at the bending test temperature of 900 °C.

3.2. Thermodynamic Analysis

Figure 11 shows the calculated binary phase diagrams of Fe–Cu, Fe–Sn, and Cu–Sn systems. All thermodynamic descriptions of the stable phases in the Fe–Cu and Fe–Sn systems were taken from the work of Shubhank and Kang[33] and Park et al.[47] respectively. As part of the development of the presented thermodynamic database, the Cu–Sn was remodeled using MQM for the

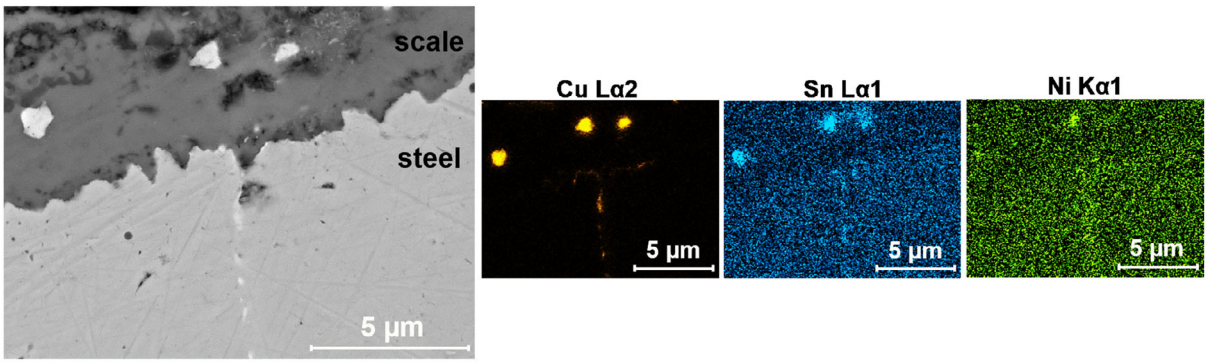

Figure 9. SEM micrograph from the interface for test no. 3 with Cu–Sn-rich phase along the grain boundary (left) and SEM/EDS for Cu, Sn, and Ni (right side).

© 2024 The Author(s). Steel Research International published by Wiley-VCH GmbH

1869344x, 0, Downloaded from https://onlinelibrary.wiley.com/doi/10.1002/srin.202400494 by Readcube (Labtiva Inc.), Wiley Online Library on [11/10/2024]. See the Terms and Conditions (https://onlinelibrary.wiley.com/terms-and-conditions) on Wiley Online Library for rules of use; OA articles are governed by the applicable Creative Commons License

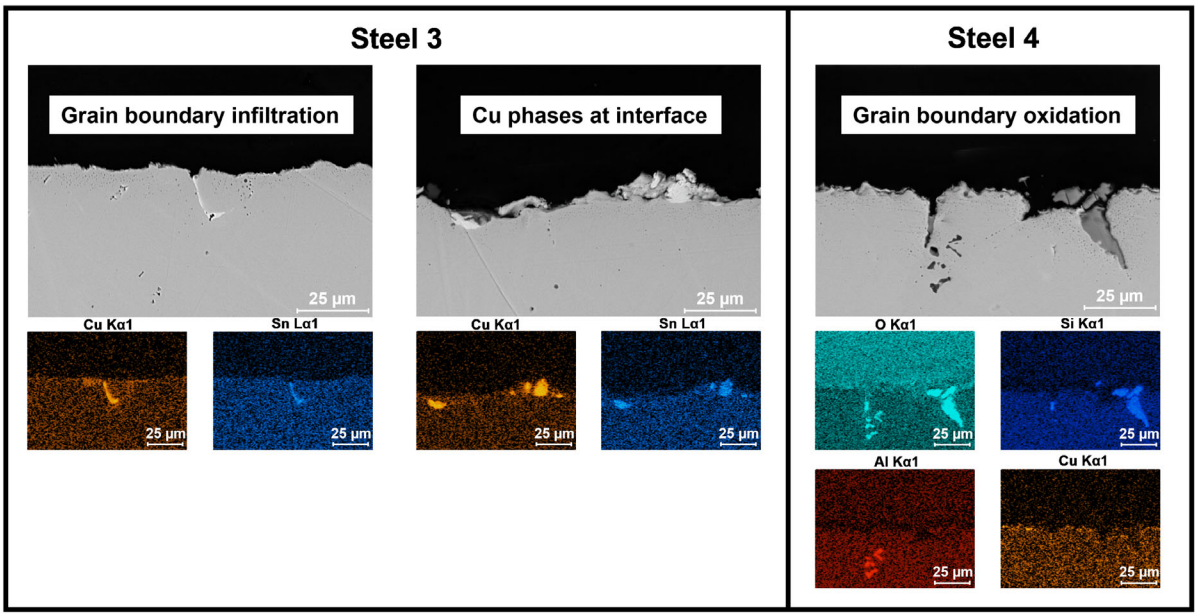

Figure 10. SEM image from the steel/scale interface with concentration mappings.

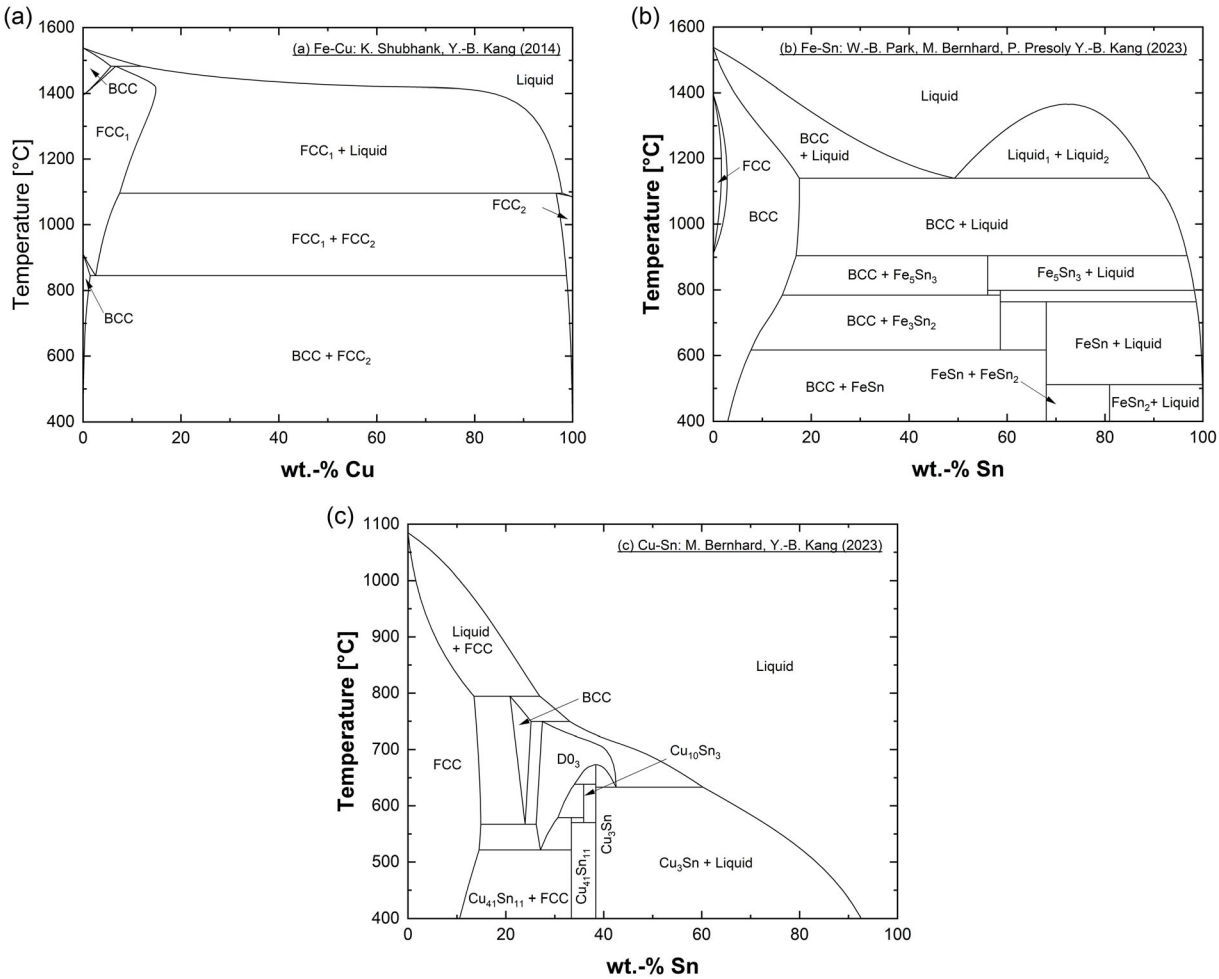

Figure 11. a) Binary phase diagrams of Fe–Cu, b) Fe–Sn, and c) Cu–Sn systems according to Shubhank and Kang,[33] Park et al.[47] and M. Bernhard and Kang,[42] respectively.

© 2024 The Author(s). Steel Research International published by Wiley-VCH GmbH

1869344x, 0, Downloaded from https://onlinelibrary.wiley.com/doi/10.1002/srin.202400494 by Readcube (Labtiva Inc.), Wiley Online Library on [11/10/2024]. See the Terms and Conditions (https://onlinelibrary.wiley.com/terms-and-conditions) on Wiley Online Library for rules of use; OA articles are governed by the applicable Creative Commons License

liquid phase,[41] with a large part of the parameters for solid phases (FCC, BCC, Cu_xSn_y, $D0_3$) corresponding to the proposal of Shim et al.[71] or slightly modified. Figure 11a shows that the solubility of Cu in FCC-Fe between 1100 and 1350 °C is high (7.5–14 wt% Cu), when the solubility limit is exceeded a Cu-rich melt is formed (90–98 wt% Cu). If the temperature drops to 900 °C, the solubility also decreases. In this range, FCC-Cu would also be stable with a certain solubility for Fe in addition to FCC-Fe. In the Fe–Sn system given in Figure 11b, Sn significantly lowers the liquidus temperature of Fe and forms a closed FCC region in the solid state, which is also known as a "γ-loop".[55,56] The FCC phase has a maximum solubility of 1.67 wt% Sn at 1167 °C. When the samples with a high Sn content (50–90 wt% Sn) are cooled, the homogeneous melt separates into a Fe-rich melt ($Liquid_1$) and a Sn-rich melt ($Liquid_2$). Complex phase equilibria can be observed between the intermetallic compounds FeSn, $FeSn_2$, Fe_3Sn_2, and Fe_5Sn_3 and liquid Sn or the Sn-rich melt. Several transitions of the stoichiometric compounds are observed. Nevertheless, Sn exerts a much more important influence in the Cu–Sn system, see Figure 11c. If a Cu-rich melt forms according to the Fe–Cu binary system, Sn would significantly lower the liquidus temperature. This means that the phase can be stable down to much lower temperatures, for example, even below 900 °C. The accumulation of Sn in the liquid therefore has an embrittling effect which, in addition to continuous casting, can also be important under hot rolling conditions.

The calculation of isothermal sections in the ternary system Fe–Cu–Sn is shown in **Figure 12**; the temperatures correspond to 900, 1100, and 1300 °C. In addition, the thermodynamic simulations are compared with the experimental literature values of Salter[31] and Ohtani et al.[32] It is shown that the concentrations of FCC and the Cu-rich melt can be predicted with sufficient accuracy. For the modeling, a ternary adjustable model parameter[42] was introduced for the liquid. To accurately predict phase stabilities and the content of Fe, Cu, and Sn in FCC and a ternary parameter was added to both solid solutions, too. At this point, however, it must be mentioned that the experimental data only describe the solid–liquid equilibrium, but an exact specification of the corresponding stable solid phases (FCC and BCC) is not given. This information is also of great importance for developing thermodynamic databases in future experimental investigations.

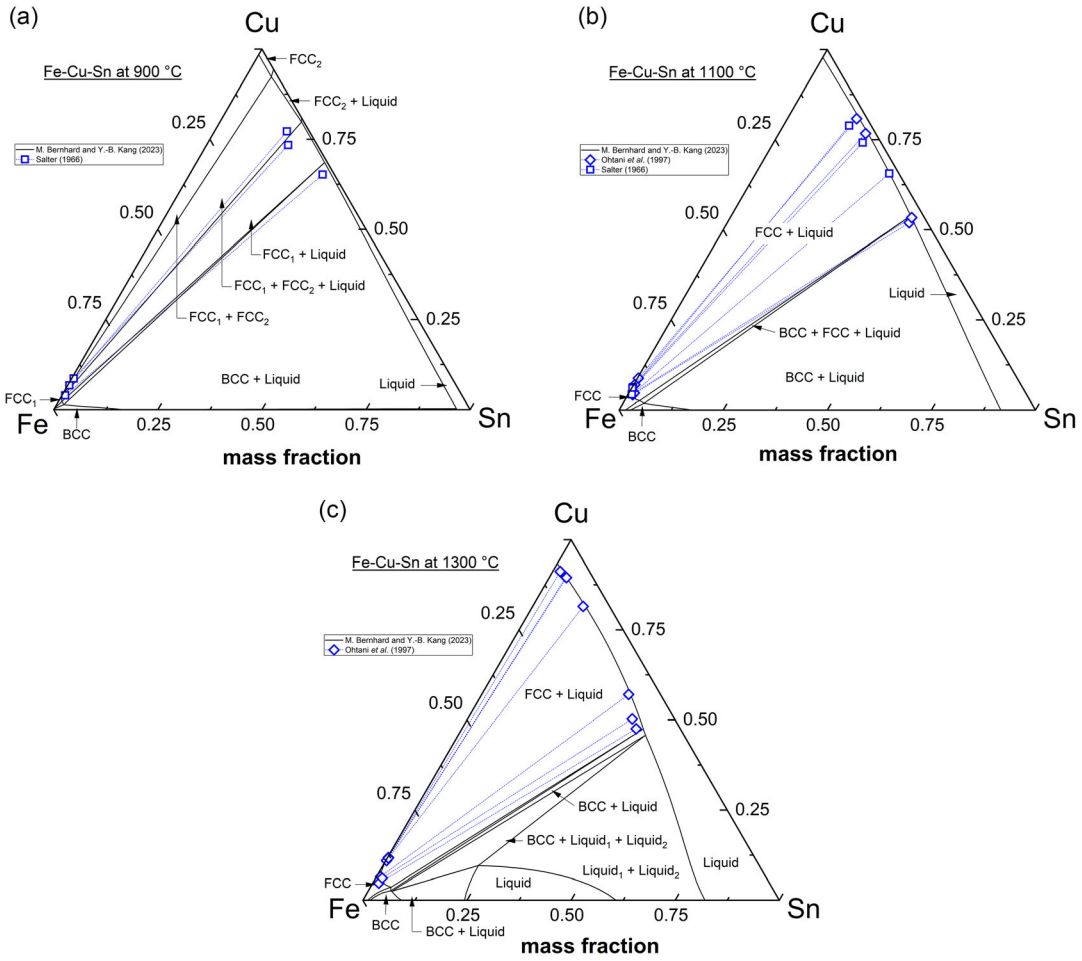

Figure 12. a) Calculated isothermal sections of the ternary system Fe–Cu–Sn at 900 °C, b) 1100 °C, and c) 1300 °C according to the model of M. Bernhard and Kang.[42] Experimental data are taken from the work of Salter[31] and Ohtani et al.[32]

© 2024 The Author(s). Steel Research International published by Wiley-VCH GmbH

1869344x, 0, Downloaded from https://onlinelibrary.wiley.com/doi/10.1002/srin.202400494 by Readcube (Labtiva Inc.), Wiley Online Library on [11/10/2024]. See the Terms and Conditions (https://onlinelibrary.wiley.com/terms-and-conditions) on Wiley Online Library for rules of use; OA articles are governed by the applicable Creative Commons License

Finally, the status of the thermodynamic database will be evaluated with a selected experiment. For this purpose, the chemical analysis of the liquid film from Figure 9 was reproduced on a laboratory scale, see also Section 2.4.

The baseline corrected DSC signal is shown in the temperature range of 750–1450 °C in **Figure 13**a. Since the DSC measurement signal corresponds qualitatively to the heat capacity curve, the calculation with the thermodynamic database was also included. In addition, Figure 13b shows the calculated phase fractions (in wt%) and the reaction integral of the DSC curve, which corresponds to the proportion of melt. The DSC signal corresponds to that of a typical peritectic transformation where two solid phases react to a liquid and a solid phase.[64] There is a clear deviation between the measurement and calculation in the value of the sharp rise at 791 °C (DSC) and 830 °C (database), which corresponds to the first time the formation of a liquid phase. The difference is about 40 °C. The first peak at 797 °C (DSC) merely marks the end of the signal; only the second peak at around 1000 °C indicates the end of the transformation. The liquidus temperature of the alloy is 1340 °C (DSC) and 1374 °C (database). To verify the DSC chart interpretation, the prepared sample was rapidly heated to 650 °C in the HT-LSCM; the temperature range of 650–900 °C was analyzed with a heating rate of 10 °C min^{-1}. Two selected micrographs obtained from the in situ HT-LSCM experiments are visualized in Figure 13c,d. The results clearly show a peritectic phase transformation and the formation of a liquid phase at 790–800 °C, confirming the previously performed DSC analysis. In general, the temperatures calculated with the database show a good agreement with the DSC measurement, but it is obvious that an extension of the experimental program is necessary to predict the stability of the liquid phase down to low temperatures (T < 800 °C).

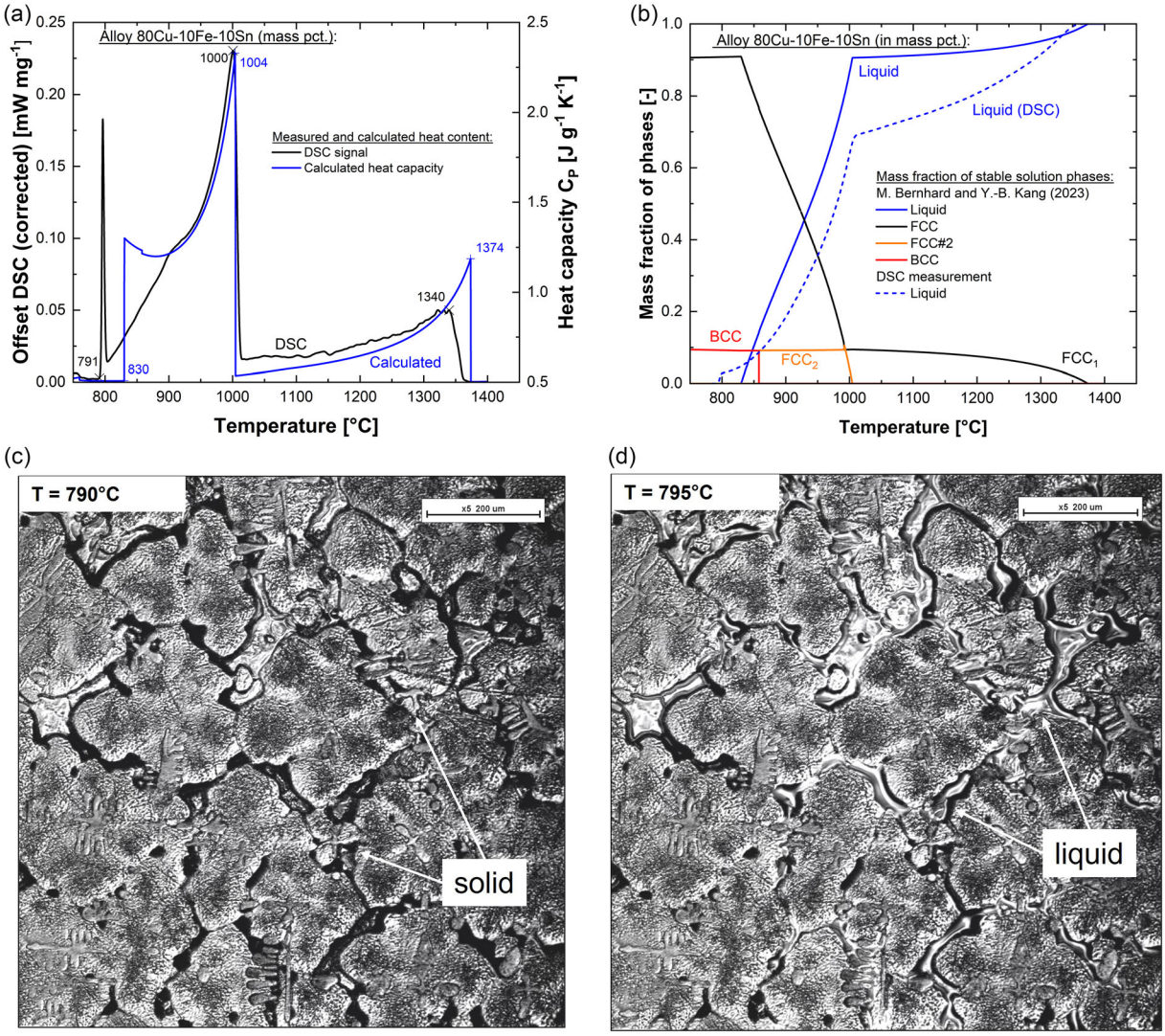

Figure 13. Phase equilibria and DSC analysis of alloy 80Cu-10Fe-10Sn (in wt%). a) Comparison between recorded DSC signal [mW mg^{-1}] and the calculated heat capacity [J $(gK)^{-1}$] between 750 and 1450 °C. b) Calculated phase fractions of liquid, BCC, FCC (Fe), and FCC#2 (Cu) according to M. Bernhard and Kang,[42] c) HT-LSCM picture at 790 °C before the peritectic phase transformation, and d) HT-LSCM picture during the peritectic phase transformation with the formation of liquid at 795 °C.

© 2024 The Author(s). Steel Research International published by Wiley-VCH GmbH

1869344x, 0, Downloaded from https://onlinelibrary.wiley.com/doi/10.1002/srin.202400494 by Readcube (Labtiva Inc.), Wiley Online Library on [11/10/2024]. See the Terms and Conditions (https://onlinelibrary.wiley.com/terms-and-conditions) on Wiley Online Library for rules of use; OA articles are governed by the applicable Creative Commons License

3.3. Mechanism of Surface Crack Formation Due to Cu and Sn Under Continuous Casting Conditions

Based on the test results presented here, the following sequence of mechanisms can be assumed for the effect of tramp elements on the formation of surface cracks during the casting and rolling of steel.

In the first step, tramp elements tend to segregate to the FCC or BCC grain boundaries. Surface segregation and grain boundary segregation were early in the focus of research, exploring the different solubility of impurities in the bulk material and at the grain boundaries and their effect on brittle fracture of materials.[72] A comprehensive overview of the state of knowledge on grain boundary segregation can be found in ref. [73] Already in 1975, Seah and Lea[74] measured equilibrium Sn-segregation on grain boundaries by Auger electron spectroscopy and deduced the thermodynamics of Sn-segregation at grain boundaries. Nachtrab and Chou[11] investigated the grain boundary segregation of Cu, Sn, and Sb at 900 °C by Auger spectroscopy. They measured a Sn-concentration of between 5.2 and 6.8 wt% for a bulk concentration of 0.031 and 0.036 wt%, indicating a grain boundary segregation by a factor of 160–180. For Cu, an initial concentration of 0.18 and 0.25 wt% led to a grain boundary concentration of 4.1 and 4.3 wt%, respectively. The enrichment by a factor of around 20 is nevertheless remarkable. Yuan et al.[75] cooled a rerolled sample to 750 °C and found a grain boundary segregation ratio of between 50 and 60 for Sn. The grain boundary segregation of Sb or As may be even higher, and the measurements of Nachtrab indicate an enrichment of Sb by a factor higher than 800.[11]

As indicated in the introduction, the segregation of elements at grain boundaries does not seem to influence the behavior in hot tensile tests significantly.[15] Oxidation of the surface at high temperatures is the decisive step in damaging the grain boundaries. High-temperature oxidation experiments show that the selective oxidation of Fe, Si, Al, and Mn results in a steadily increasing segregation of Cu and Sn at the steel/scale interface and along grain boundaries. If the solubility limit is finally exceeded, a Cu- and Sn-rich phase may form. Ni plays a decisive role in increasing the solubility of Cu. Ni reduces the oxidation rate at temperatures above 900 °C,[70] thus favoring internal oxidation, namely, grain boundary oxidation. The role of Ni is positive with respect to the suppression of the formation of a Cu-rich phase but nevertheless does not prevent the damage of grain boundaries and the subsequent growth of defects along the grain boundaries. Ni should not be misunderstood as a panacea against surface cracking. The experimental results indicate that the gas atmosphere and the cooling or heating strategy may help to control the influence of elevated content of tramp elements as already demonstrated for thin slab casting and direct rolling processes.[30]

The thermodynamic understanding of the system Fe–Cu–Sn is sufficiently accurate to calculate the solubility limit for Cu and Sn in FCC and to predict the melting point of the resulting Cu- and Sn-rich phases. The CALPHAD results could be confirmed by means of DSC measurements and HT-LSCM. The existence of liquid phases along the FCC grain boundaries at temperatures below 900 °C is nevertheless astonishing. For other tramp elements, such as Sb or As, the thermodynamic data indicate even lower eutectic temperatures, but measurements are so far rare. The need for future work in this field is evident.

The assumed sequence of mechanisms finally leading to surface crack formation in casting is confirmed by IMC-B tests at 900 °C. The significance of the proposed formulae by Wolf[14] and Melford[7] for calculating an equivalent Cu content is surprisingly clear, and the critical Cu-equivalent is for the present testing conditions determined with appr. 0.2 and thus slightly lower than expected. It is important to note that the Cu-equivalent is only meaningful if both Cu and Sn are present in the steel. IMC-B-tests at 900 °C show that neither Cu nor Sn have a negative effect on defect formation if they are contained in the steel alone. The addition of Ni reduces the sensitivity toward the formation of surface cracks significantly, and steel with a Cu-equivalent below 0.1 behaves very similarly to the reference steel grade without the additions of tramp elements. So far, these results for 900 °C are unique. Further work will focus on the influence of Cu, Sn, and Ni at other bending temperatures and cooling under different gas atmospheres and cooling strategies.

4. Conclusion

The understanding of the role of Cu and Sn in the formation of surface defects in casting and rolling goes back to the 1960s. In early works, Melford[7] and Wolf[14] proposed a Cu-equivalent to predict a critical limit of Cu and Sn in casting processes. The presumed effect of liquid metal embrittlement has always been assumed but never quantified in experiments.

The present work deals with results from an in situ bending test, clearly showing the limits of Cu and Sn content with respect to surface cracking in casting processes. The beneficial role of Ni is also clearly visible. The experimental results were cross-checked with the results of high-temperature oxidation experiments, confirming the role of tramp elements and indicating the importance of gas atmosphere and temperature control in damaging grain boundaries. Thermodynamic data provide information on grain boundary segregation and solubility limits in the systems Fe–Cu–Sn–Ni. The results were confirmed by thermal analysis and high-temperature confocal investigations.

The results show that contrary to previous assumptions, the elements Cu and Sn also have a negative effect at temperatures of 900 °C, which was previously attributed to the temperature range of around 1100 °C. The results also indicate that adding Ni is beneficial and that the negative impact of the tramp elements might be controlled by the surrounding gas atmosphere and temperature control.

Acknowledgements

C.B., M.B., M.K., and P.P. gratefully acknowledge the financial support under the scope of the COMET program within the K2 Center "Integrated Computational Material, Process and Product Engineering (IC-MPPE)" (Project No 886385). This program is supported by the Austrian Federal Ministries for Climate Action, Environment, Energy, Mobility, Innovation and Technology (BMK) and for Labour and Economy (BMAW), represented by the Austrian Research Promotion Agency (FFG), and the Federal States of Styria, Upper Austria and

© 2024 The Author(s). Steel Research International published by Wiley-VCH GmbH

1869344x, 0, Downloaded from https://onlinelibrary.wiley.com/doi/10.1002/srin.202400494 by Readcube (Labtiva Inc.), Wiley Online Library on [11/10/2024]. See the Terms and Conditions (https://onlinelibrary.wiley.com/terms-and-conditions) on Wiley Online Library for rules of use; OA articles are governed by the applicable Creative Commons License

Tyrol. This research was supported by the Brain Pool program funded by the Ministry of Science and ICT through the National Research Foundation of Korea (NRF-2022H1D3A2A01081708).

J.W. and G.G. gratefully acknowledge the funding support of K1-MET GmbH, metallurgical competence center. The research program of the K1-MET competence center is supported by COMET (Competence Center for Excellent Technologies), the Austrian program for competence centers. COMET is funded by the Federal Ministry for Climate Action, Environment, Energy, Mobility, Innovation and Technology, the Federal Ministry for Labour and Economy, the Federal States of Upper Austria, Tyrol and Styria as well as the Styrian Business Promotion Agency (SFG) and the Standortagentur Tyrol. Furthermore, Upper Austrian Research GmbH continuously supports K1-MET.

Conflict of Interest

The authors declare no conflict of interest.

Data Availability Statement

Research data are not shared.

Keywords

in situ bending tests, intergranular oxidation, surface defects in continuous casting, thermodynamics of the system Fe–Cu–Sn, tramp elements

Received: June 17, 2024
Revised: August 8, 2024
Published online:

[1] V. Leroy, *Effects of Tramp Elements in Flat and Long Products: Final Report*, Office for Official Publications of the European Communities, Luxembourg **1995**.
[2] J. C. Herman, V. Leroy, in *Conf. on Metal Working and Steel Processing*, Cleveland **1996**, p. 15.
[3] H. Matsuoka, K. Osawa, M. Ono, M. Ohmura, *ISIJ Int.* **1997**, *37*, 255.
[4] T. Yamada, M. Oda, O. Akisue, *Tetsu to Hagane* **1997**, *37*, 255.
[5] O. Rod, C. Becker, M. Nylén, *Jernkontorets Forskning* **2006**, *D 819*, 1.
[6] D. A. Melford, *J. Iron Steel Inst.* **1966**, *204*, 495.
[7] D. A. Melford, *Philos. Trans. R. Soc. Lond. A: Math. Phys. Sci.* **1980**, *295*, 89.
[8] R. Kiessling, *Met. Sci.* **1980**, *14*, 161.
[9] M. Wolf, *Trans. Iron Steel Inst. Jpn* **1984**, *24*, 351.
[10] M. M. Wolf, H. Schwabe, *On Tramp Element Control in Electric Steelmaking*, Associazione Italiana di Metallurgia, Florence, Italy **1986**.
[11] W. T. Nachtrab, Y. T. Chou, *J. Mater. Sci.* **1984**, *19*, 2136.
[12] W. T. Nachtrab, Y. T. Chou, *Metall. Trans. A* **1988**, *19*, 1305.
[13] Y. Zou, E. W. Langer, *Mater. Sci. Eng. A* **1989**, *110*, 203.
[14] M. M. Wolf, *Continuous Casting. Volume 9, Initial Solidification and Strand Surface Quality of Peritectic Steels*, Iron and Steel Society, Warrendale **1997**.
[15] O. Comineli, A. Qaban, B. Mintz, *Metals* **2022**, *12*, 1671.
[16] H. Peng, W. Chen, L. Chen, D. Guo, *High Temp. Mater. Process.* **2015**, *34*, 19.
[17] N. Imai, N. Komatsubara, K. Kunishige, *ISIJ Int.* **1997**, *37*, 217.
[18] K. Shibata, S.-J. Seo, M. Kaga, H. Uchino, A. Sasanuma, K. Asakura, C. Nagasaki, *Mater. Trans.* **2002**, *43*, 292.
[19] R. Krobath, C. Bernhard, in *AISTech Proc.*, Nashville, USA **2017**, pp. 1827–1837.
[20] R. Krobath, C. Bernhard, *Steel Res. Int.* **2020**, *76*, 2000234.
[21] R. Krobath, C. Bernhard, S. Ilie, J. Six, S. Hahn, P. Pennerstorfer, *Berg- und Hüttenmannische Monatshefte* **2019**, *164*, 461.
[22] M. Krobath, R. Krobath, C. Bernhard, W. Ecker, *Materials* **2020**, *13*, 2281.
[23] R. Krobath, C. Bernhard, in *10th ECCC European Conf. on Continous Casting*, Bari, Italy, Associazione Italiana di Metallurgia **2021**.
[24] G. Gaiser, R. Krobath, P. Presoly, C. Bernhard, *J. Mater. Res. Technol.* **2023**, *26*, 9276.
[25] G. Gaiser, P. Presoly, C. Bernhard, *Metals* **2023**, *13*, 892.
[26] P. Krajewski, R. Krobath, C. Bernhard, J. Miettinen, S. Louhenkilpi, S. Ilie, T. Schaden, *Berg- und Hüttenmännische Monatshefte* **2015**, *160*, 109.
[27] M. Bernhard, G. Santos, L. Preuler, M. Taferner, G. Wieser, J. Laschinger, S. Ilie, C. Bernhard, *Steel Res. Int.* **2022**, *93*, 12.
[28] B. Mintz, D. N. Crowther, *Int. Mater. Rev.* **2010**, *55*, 168.
[29] E. S. Szekeres, in *Proc. of the 6th Inter. Conf. on Clean Steel*, Balatonfüred, Hungary **2002**, pp. 324–338.
[30] G. Gaiser, P. Presoly, C. Bernhard, K. Baumgartner, S. Grosseiber, *ISIJ Int.* **2024**, https://doi.org/10.2355/isijinternational.ISIJINT-2024-072.
[31] W. Salter, *J. Iron Steel Inst.* **1967**, *205*, 1156.
[32] H. Ohtani, H. Suda, K. Ishida, *ISIJ Int.* **1997**, *37*, 207.
[33] K. Shubhank, Y.-B. Kang, *Calphad* **2014**, *45*, 127.
[34] P. J. Spencer, *Calphad* **2008**, *32*, 1.
[35] C. W. Bale, E. Bélisle, P. Chartrand, S. A. Decterov, G. Eriksson, A. E. Gheribi, K. Hack, I.-H. Jung, Y.-B. Kang, J. Melançon, A. D. Pelton, S. Petersen, C. Robelin, J. Sangster, P. Spencer, M.-A. van Ende, *Calphad* **2016**, *54*, 35.
[36] H.-L. Chen, Y. Du, H. Xu, W. Xiong, *J. Mater. Res.* **2009**, *24*, 3154.
[37] C. Servant, B. Sundman, O. Lyon, *Calphad* **2001**, *25*, 79.
[38] S. Cui, I.-H. Jung, *Calphad* **2017**, *56*, 241.
[39] J. Miettinen, *Calphad* **2008**, *32*, 500.
[40] M. Bernhard, W.-B. Park, Y.-B. Kang, S. Ilie, C. Bernhard, in *6th ESTAD - European Steel Technology and Application Days*, Düsseldorf, Germany **2023**.
[41] M. Bernhard, W.-B. Park, P. Presoly, Y.-B. Kang, in *Proc. of 50th Inter. Conf. on Computer Coupling of Phase Diagrams and and Thermochemistry (CALPHAD L)*, Boston, USA **2023**.
[42] M. Bernhard, Y.-B. Kang, *Unpublished research*, **2023**.
[43] A. D. Pelton, S. A. Degterov, G. Eriksson, C. Robelin, Y. Dessureault, *Metall. Mater. Trans. B* **2000**, *31*, 651.
[44] A. D. Pelton, P. Chartrand, *Metall. Mater. Trans. A* **2001**, *32*, 1355.
[45] A. D. Pelton, Y.-B. Kang, *Int. J. Mater. Res.* **2007**, *98*, 907.
[46] M.-S. Kim, Y.-B. Kang, *Calphad* **2015**, *51*, 89.
[47] W.-B. Park, M. Bernhard, P. Presoly, Y.-B. Kang, *J. Mater. Inf.* **2023**, *3*, 5.
[48] P. Waldner, A. Pelton, *J. Phase Equilib. Diffus.* **2005**, *26*, 23.
[49] M. Bernhard, Y.-B. Kang, P. Presoly, A. E. Gheribi, C. Bernhard, *Calphad* **2020**, *70*, 101795.
[50] Michael Bernhard, Won-Bum Park, Youn-Bae Kang, *Calphad* **2023**, *83*, 102622.
[51] P. Chartrand, A. D. Pelton, *J. Phase Equilib. Diffus.* **2000**, *21*, 141.
[52] M. Hillert, The Compound Energy Formalism, *J. Alloys Compd.* **2001**, *320*, 161.
[53] M. Hillert, M. Jarl, *Calphad* **1978**, *2*, 227.
[54] B. Sundman, J. Ågren, *J. Phys. Chem. Solids* **1981**, *42*, 297.
[55] M. Bernhard, P. Presoly, N. Fuchs, C. Bernhard, Y.-B. Kang, *Metall. Mater. Trans. A* **2020**, *51*, 5351.
[56] M. Bernhard, N. Fuchs, P. Presoly, P. Angerer, B. Friessnegger, C. Bernhard, *Mater. Charact.* **2021**, *174*, 111030.

© 2024 The Author(s). Steel Research International published by Wiley-VCH GmbH

1869344x, 0, Downloaded from https://onlinelibrary.wiley.com/doi/10.1002/srin.202400494 by Readcube (Labtiva Inc.), Wiley Online Library on [11/10/2024]. See the Terms and Conditions (https://onlinelibrary.wiley.com/terms-and-conditions) on Wiley Online Library for rules of use; OA articles are governed by the applicable Creative Commons License

[57] M. Bernhard, P. Presoly, C. Bernhard, S. Hahn, S. Ilie, *Metall. Mater. Trans. B: Process Metall. Mater. Process. Sci.* **2021**, *52*, 2821.
[58] W. J. Boettinger, U. R. Kattner, K.-W. Moon, *NIST Recommend. Pract. Guide* **2006**, 1.
[59] M. Kern, M. Bernhard, C. Bernhard, Y.-B. Kang, *Scr. Mater.* **2023**, *230*, 115431.
[60] M. Kern, M. Bernhard, Y.-B. Kang, C. Bernhard, *Acta Mater.* **2024**, *269*, 119826.
[61] C. Bernhard, M. Kern, M. Bernhard, *Steel Res. Int.* **2023**, https://doi.org/10.1002/srin.202300547.
[62] M. Liu, M. Bernhard, M. Kawuloková, J. Walek, M. Kern, S. Zlá, P. Presoly, B. Smetana, M. Tkadlečková, G. Xu, Y.-B. Kang, C. Bernhard, *J. Mater. Res. Technol.* **2023**, *24*, 3534.
[63] S.-C. Moon, D. Phelan, R. Dippenaar, *Mater. Charact.* **2021**, *172*, 110841.
[64] P. Presoly, R. Pierer, C. Bernhard, *Metall. Mater. Trans. A* **2013**, *44*, 5377.
[65] S. Feichtinger, S. K. Michelic, Y.-B. Kang, C. Bernhard, *J. Am. Ceram. Soc.* **2014**, *97*, 316.
[66] S. K. Michelic, J. Goriupp, S. Feichtinger, Y.-B. Kang, C. Bernhard, J. Schenk, *Steel Res. Int.* **2016**, *87*, 57.
[67] S. S. Jung, I. Sohn, *Metall. Mater. Trans. B* **2012**, *43*, 1530.
[68] J. Cejka, S. K. Michelic, *Metals* **2023**, *13*, 686.
[69] Ľ. Drozdová, B. Smetana, P. Presoly, V. Novák, M. Machů, M. Bernhard, H. Francová, S. Zlá, L. Řeháčková, C. Bernhard, *J. Therm. Anal. Calorim.* **2020**, *142*, 535.
[70] G. Gaiser, P. Presoly, C. Bernhard, *High-temperature oxidation of steel recycled from scrap: The role of tramp elements and their influence on oxidation behavior.* ESTAD (European Steel Technology and Application Days), Düsseldorf, Germany **2023**, p. 9.
[71] J.-H. Shim, C.-S. Oh, B.-J. Lee, D. N. Lee, *Int. J. Mater. Res.* **1996**, *87*, 205.
[72] M. Paju, R. Möller, *Scr. Metall.* **1984**, *18*, 813.
[73] P. Lejcek, *Grain Boundary Segregation in Metals*, Springer, Berlin **2010**.
[74] M. P. Seah, C. Lea, *Philos. Mag.: J. Theor. Exp. Appl. Phys.* **1975**, *31*, 627.
[75] Z.-X. Yuan, J. Jia, A.-M. Guo, D.-D. Shen, S.-H. Song, *Scr. Mater.* **2003**, *48*, 203.

© 2024 The Author(s). Steel Research International published by Wiley-VCH GmbH

1869344x, 0, Downloaded from https://onlinelibrary.wiley.com/doi/10.1002/srin.202400494 by Readcube (Labtiva Inc.), Wiley Online Library on [11/10/2024]. See the Terms and Conditions (https://onlinelibrary.wiley.com/terms-and-conditions) on Wiley Online Library for rules of use; OA articles are governed by the applicable Creative Commons License